CRYSTAL GROWTH & DESIGN
2005
VOL. 5, NO. 6
2139−2145

Orientation and Mg Incorporation of Calcite Grown on Functionalized Self-Assembled Monolayers: A Synchrotron X-ray Study

Seo-Young Kwak and Elaine DiMasi*

National Synchrotron Light Source, Brookhaven National Laboratory, Upton, New York 11973-5000

Yong-Jin Han† and Joanna Aizenberg

Bell Laboratories, Lucent Technologies, Murray Hill, New Jersey 07974

Ivan Kuzmenko

Advanced Photon Source, Argonne National Laboratory, Argonne, Illinois 60439

Received April 19, 2005

ABSTRACT: Calcite crystals were nucleated from $MgCl_2/CaCl_2$ solutions onto functionalized self-assembled monolayers adsorbed onto E-beam evaporated Au films. Synchrotron X-ray scattering studies of the crystals reveal new information about preferred orientation and Mg incorporation. The Au [111] axis is distributed within 2.6° of the film surface normal, but the oriented crystals may be tilted up to 6° away from this axis. For low Mg^{2+} content, SO_3^--functionalized films nucleated primarily near the (106) calcite face, odd-chain-length carboxylic acid terminated alkanethiol films nucleated near the (012) face, and even-chain-length carboxylic acid terminated alkanethiol films nucleated near the (113) face. $[Mg^{2+}]/[Ca^{2+}]$ concentration ratios (n) of 2 and greater defeated this preferred orientation and created a powder texture. Diffraction patterns within the layer plane from the coarse calcite powders indicated a shift to higher 2θ accompanied by peak broadening with increasing n. For $0.5 < n < 3.5$, a double set of calcite peaks is observed, showing that two distinct Mg calcite phases form: one of comparatively lower Mg content, derived from the templated crystals, and a Mg-rich phase derived from amorphous precursor particles. According to the refinement of lattice parameters, Mg incorporation of up to 18 mol % occurs for $n = 4$, independent of film functionality. We discuss the differences between the differently functionalized monolayers and also introduce the hypothesis that two separate routes to Mg calcite formation occur in this system.

I. Introduction

Low-temperature magnesian calcites are key to a complete understanding of seawater chemistry, the global carbonate cycle, and the biological mineralization of many marine organisms. Recently, Mg calcites have been suggested as a new route to synthetic microstructured composite materials,[1] inspired by those same marine biominerals. Through the use of synthetic organic templates, in vitro Mg calcite precipitates exhibit characteristic morphologies. This suggests a degree of control over mineralization which may be useful for development of novel ceramic−polymer materials.

However, unresolved problems in Mg/Ca carbonate chemistry are numerous, despite decades of research. Part of the complexity lies in the many environmental factors which influence carbonate precipitation. The carbon dioxide partial pressure of the air in equilibrium with the water reservoir, together with the ionic content, pH, and temperature, must be known if the concentration of $[CO_3^{2-}]$ is to be controlled. It has been shown that the concentration of carbonate directly affects the Mg/Ca ratio in the calcite shells of planktonic foraminifera cultured in laboratory.[2] Paleothermometry has relied heavily upon measured Mg/Ca ratios in such marine organisms, which incorporate $\sim 10^{-2}$ mol of Mg/mol of Ca in $CaCO_3$. The temperature calibrations for these proxies are under continual revision as better measurement methods and controls are developed.[3−5]

High-Mg calcites (4−20 mol % Mg) are also found, as both nonskeletal and biomineral precipitates.[6] Variation of the Mg/Ca ratio in seawater, from ~1 to the present value of 5.2 on time scales of approximately 10^8 years, has resulted in varying Mg content of calcium carbonates. In laboratory culture, calcite shells of coralline algae have been shown to reflect the Mg content of the ambient seawater, and these simple biomineralizers have been contrasted with those which exert more control over calcite mineralization and therefore more independence from the environment.[6] The high-Mg calcite biominerals seem especially relevant to the organic-templated Mg calcites mentioned above, for two reasons: they contain enough Mg to affect crystal size and shape and there is the potential for an organic template or matrix to override the dictates of the ambient Mg/Ca ratio.

Disentangling the effects of Mg^{2+} in solution from those of an organic matrix, even a simplified one, requires careful experimental procedures. As mentioned above, there are many thermodynamic quantities to consider. $CaCO_3$ can be obtained as any of several polytypes which kinetically compete with each other.[7]

* To whom correspondence should be addressed. E-mail: dimasi@bnl.gov.
† Present address: Lawrence Livermore National Laboratory, Livermore, CA 94551.

10.1021/cg050164x CCC: $30.25
Published on Web 07/27/2005

It has been long recognized that Mg in laboratory solutions and in seawater inhibits the growth of pure calcite, leading to precipitation of either the aragonite polytype of $CaCO_3$ or magnesian calcites in which Mg substitutes at random Ca sites, decreasing the calcite lattice parameters.[7] Mg interacts strongly with several calcite crystal surfaces,[8,9] and yet, it has also been shown in simulations that Mg energetically prefers bulk rather than surface sites in the ordered $CaMg(CO_3)_2$ mineral dolomite.[10] Differential Mg incorporation at step edges also leads to intrasectoral zoning of Mg into calcite,[11] as recent AFM studies have discussed.[12]

Can the specification of an organic template actually overcome all of these variables and produce crystals of finely controlled shape, crystal structure, and composition? Recent experiments have addressed this question with calcite and Mg calcite nucleation at self-assembled organic monolayers (SAMs): particularly, long-chain mercapto−alcohols, −carboxylic acids, and −sulfonic acids on Au (111) surfaces.[1,13] These SAMs produce oriented crystals which nucleate with a different preferred face against each distinct film. These crystals were characterized by electron microscopy and laboratory X-ray diffraction to evaluate their morphology and to confirm the calcite polytype. With Mg as a growth modifier, added to the solution in $[Mg^{2+}]/[Ca^{2+}]$ ratios from 0.5 to 4.0, crystals grow in a more rounded morphology, making it impossible to assess by scanning electron microscopy whether the preferred orientation is retained. Because dependence on the choice of SAM is still observed, the experiments suggest that an organic template and a soluble modifier can together control crystal morphology. Whether the molecules in the template act by direct structural registry or stereochemical recognition with the crystal face, by creating a charged surface compatible with the energetics of the preferred face, or by affecting cation gradients (and hence kinetics) in solution remains to be discovered.

High-resolution structural measurements are required to scrutinize the relationship between the mineral and film. This paper presents a synchrotron X-ray scattering study of Mg calcite crystals nucleated on three different SAMs grown on Au films. Crystal orientation determined from rocking curves on calcite Bragg peaks is compared with the underlying substrate texture of the Au. Our measurements show that because of the mismatch between Au, SAM, and Mg calcite grain sizes, direct structural correlations between them are unlikely. From refinement of the calcite lattice parameters, the amount of Mg incorporation is quantified for each of eight runs with $[Mg^{2+}]/[Ca^{2+}]$ ratios varying from 0 to 4. At low Mg concentrations, the diffraction patterns show that calcite coexists with Mg calcite. Smaller crystals of more monodisperse Mg calcite are observed at the highest Mg concentrations. This Mg incorporation pattern is independent of SAM type. We conclude that, in this system, the nucleating template is not sufficient to control Mg content in precipitated calcite.

II. Experimental Details

A. Sample Preparation. SAMs were prepared by soaking 500 nm gold films, which were E-beam evaporated on Si(100) wafers primed with 2 nm Ti layers, in 5 mM solutions of $HS-(CH_2)_{10}-CO_2H$, $HS-(CH_2)_{15}-CO_2H$, and $HS-(CH_2)_{11}-SO_3H$ in ethanol for a minimum of 6 h.[14] Calcium carbonate precipitation on the SAMs was performed as described in previous literature, by exposing aqueous solutions of $CaCl_2$ and $MgCl_2$ to vapors from $(NH_4)HCO_3$(s) solid salt.[15,16] Magnesium to calcium ratios, n ($n = [Mg^{2+}]/[Ca^{2+}]$), were varied from 0 to 4 with an increment of 0.5. The crystallization took place inside a desiccator at room temperature for 2 h. Each individual solution was contained in a separate well of a well plate so that all substrates were mineralized together in the same environment. Each substrate was then rinsed with H_2O and dried with compressed N_2. The complete set of samples consists of three series, functionalized with odd-chain-length carboxylic acid (C15 films), even-chain-length carboxylic acid (C10 films), or sulfonic acid (SO3 films). Each series contains eight films nucleated with different $[Mg^{2+}]/[Ca^{2+}]$ solution ratios.

B. Synchrotron X-ray Methods. Measurements were made at the National Synchrotron Light Source, beamline X22A, using an X-ray wavelength of 1.208 Å. A Soller collimator was placed before a Bicron scintillator detector for a resolution of 0.045° in scattering angle. Samples were measured in air both in a reflection geometry, with an illuminated spot size of 0.5×0.4 mm^2, and at a grazing incident angle of 0.5°, which spreads the illuminated beam into a stripe 0.5 mm wide running the length of the sample (10−20 mm). In the latter case samples were rocked azimuthally by 1 or 2° during the scans. Measured peak intensities over the course of a few hours' measurement remained consistent, implying that no X-ray damage to the calcite took place. Selected samples were remeasured at NSLS beamline X6B with wavelength 0.65 Å, using a Ge(111) analyzer crystal for high-resolution measurement of peak widths with coherence length ~300 nm.

It is expected that X-ray damage to the underlying alkanethiol monolayer will occur under these conditions. In a separate study, we attempted to measure X-ray reflectivity from C15 and C10 monolayers on identical Au films which had not been exposed to a crystallizing solution; those measurements were performed with the sample under a helium atmosphere and with beam attenuators inserted before the sample over most of the q range sampled. We found that these films were structurally so disordered that little information could be obtained, in contrast to previous publications of the same molecules on single-crystal Au substrates.[17] These measurements, performed at the CMC-CAT liquid spectrometer at the Advanced Photon Source, are presented as Supporting Information with this publication. We believe that the disorder in the SAM is related to the unfavorable texture of the Au, which is discussed below.

III. Results

A. SEM Images. SEM images of these samples provide an overview of morphogenesis for calcites with Mg incorporation (Figure 1). At $n = 0$, rhombohedral calcite particles show a distinctive preferred orientation, which is different for each SAM. As the Mg content increases, the particle shape is changed to round off all edges and to elongate the shape, especially on the C10 and C15 films. Eventually, much smaller, spherical particles are formed. In case of calcite on SO3 film, faceted crystals appear until $n = 1.0$; crystals are less elongated and eventually also become spherical. Overall, the increase of the concentration of Mg^{2+} ions reduces the particle size from 10−20 to 0.5−2 μm. At $n = 4$, no matter what kind of functional group or chain length the SAM has, the particles are apparently identical. The spherical shape results from formation of an amorphous calcium carbonate precursor phase, as we confirmed previously with infrared and Raman spectroscopy (see ref 1 and references therein). Because of the spherical shape, X-ray methods are required to provide informa-

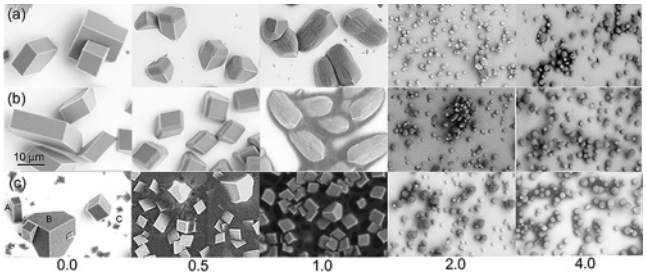

Figure 1. SEM micrographs of calcite crystals on different organic templates in the presence or absence of Mg ions: (a) C15 film; (b) C10 film; (c) SO3 film. Each micrograph is the same scale, and the bar indicates 10 μm. From left to right, $[Mg^{2+}]/[Ca^{2+}] = n = 0.0$, 0.5, 1.0, 2.0, and 4.0, respectively. For SO3 films with $n = 0.0$, the relative occurrences of three morphologies (labeled A−C) as shown are representative of the entire sample.

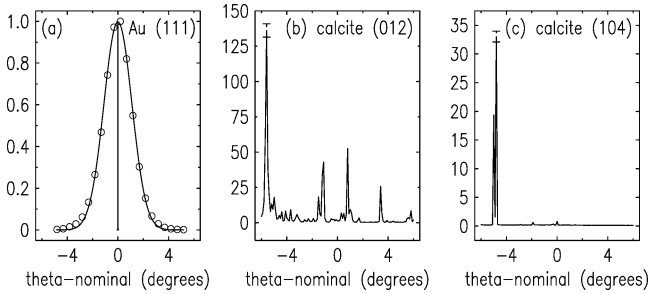

Figure 2. Rocking curves showing the angular distributions of Au and calcite crystals: (a) Au (111) peak (open circles), with fit curve (line) and Si (004) peak (thin line); (b) C15 film, $n = 0.0$ about calcite (012) peak; (c) C15 film, $n = 0.0$ about calcite (104) peak.

tion about the polytype or orientation of these particles when they ultimately crystallize.

B. Film Texture: Angular Distributions and Sizes of Crystal Domains. X-ray scattering, unlike SEM, is sensitive to details of the film texture. We observed broad Au (111) Bragg peaks, and this indicates disorder in the Au substrate domains. As reported previously, the films are aligned with the [111] axis along the surface normal and there is no orientational order within the film plane.[15] However, the angular spread of [111] axes of the Au grains has a full width of 2.6° about the surface normal, as shown by the rocking curve in Figure 2a (open circles and fit curve). The resolution-limited 0.014° full width measured from the Si substrate (004) peak is shown for comparison (thin line). In contrast, peaks from the calcite crystals are relatively sharp and have coarse distributions in sample tilt. We measured a selection of calcite Bragg peaks in the range ±6° about the surface normal to judge the degree of preferred orientation. Figure 2b shows calcite (012) peaks from crystals nucleated on a C15 monolayer in the absence of Mg^{2+} ($n = 0$). A significant cluster of peaks near the surface normal is present in the rocking curve. This texture corresponds to the (012) nucleation identified previously from electron microscopy.[15] Note, however, that the calcite peaks show no sign of the 2.6° wide center of mass that the Au film shows. This measurement makes it clear that the registry between the Au grains and the calcite face, and by implication the organic monolayer between them, cannot be exact. Rather than being structurally templated at the molecular level, the faces of the relatively large calcite crystals only approximately span the layer plane of the Au film and SAM.

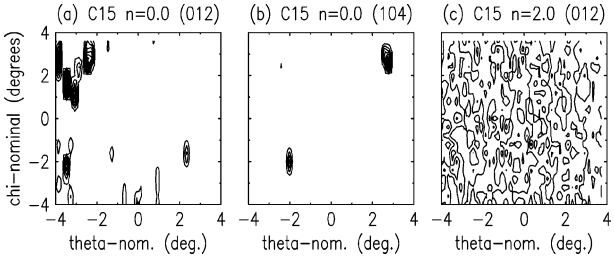

Figure 3. Pole figures for (a) the sample of C15 film with $n = 0$ about the (012) peak, (b) the sample of C15 film with $n = 0$ about the (104) peak, and (c) the sample of the C15 film with $n = 2$ about the (012) peak. These typify oriented, stray, and no orientation, respectively.

Even in these textured films, crystals may happen to fall upon the surface in other orientations. We refer to these as stray crystals, since they can occur with equal probability regardless of SAM type, and they are much less numerous than the oriented crystals. For example, (104) peaks are often observed near the surface normal under different preparation conditions, simply because this is a strong X-ray scattering peak and an energetically favorable face that is expressed when calcite nucleates homogeneously from solution. The signature in the rocking curves for C15 with $n = 0$ is shown in Figure 2c. To make the most complete assessment of the series of films, partial pole figures were examined. Examples of these dual-rocking-curve measurements are shown as contour plots in Figure 3. Figure 3a shows the oriented calcite (012) texture on the C15, $n = 0$ film. Each spot comes from a different calcite crystal in the beam, and aside from being grouped near the origin, they bear no relation to one another. The stray (104) nucleation is shown in Figure 3b. The absence of surface normal peaks shows as a flat background level in the pole figure (Figure 3c).

C. Calcite Crystal Texture Measurements. Using the above methods to assess calcite crystal orientation, we can make some general statements about the system. Samples studied by rocking curves and pole figures are summarized in Table 1, where O indicates oriented crystals, s refers to stray crystals, and n indicates no evidence for surface-normal alignment. Blank entries denote combinations which were not measured. The orientation differs with different SAM functionality. We first consider the series of C15 films. Preferred nucleation within a few degrees of the (012) plane is observed at low Mg^{2+} levels, consistent with previous reports.[1] At the molar ratio $n = 2$, diffraction patterns show no orientational texture. Stray crystals in the (104) orientation become less numerous as n increases and also disappear for $n > 2$. Hence, Mg interferes with the effects of the SAM surface and disrupts the expression of energetically stable calcite planes, at the same time. The C10 films exhibit stray orientations when (012) and (104) peaks are investigated. Instead, the (113) peak clearly appears on C10 film, although proximity to the Au (111) peak creates a high background level. For $n > 1$, the orientation is again disrupted, but with a subtle difference compared to that for C15. The table entries show that the

Table 1. Assessment of $\theta-\chi$ Rocking Curves Measured for Selected Mg Concentrations for Each Headgroup, Measured at the Indicated Bragg Peaks[a]

	n	[012]	[104]	[116]	[006]	[113]
C15	0	O	O/s			n
C15	0.5	O	O/s			
C15	1.0	O	O/s			
C15	2.0	n	s			
C15	4.0	n	n			
C10	0	n	O			O
C10	0.5	O/s	s			O[b]
C10	1.0	O/s	O/s			*b*
C10	2.0	n	O/s			n
C10	4.0	n	n			n
SO3	0	n	s	O	n	n
SO3	0.5	n	O/s	O/s	O/s	
SO3	1.0	n	s	O/s	O	
SO3	2.0	n	n	n	n	
SO3	4.0	n	n	n	n	

[a] Legend: O = oriented about the surface normal; s = stray crystallites with surface-normal orientation; n = no peaks observed. Blank cells indicate that the given peak was not scanned. [b] The (113) peak intensity quickly disappears into the overlapping Au (111).

orientation of calcite on C15 film is constant until it vanishes, while the calcite particles of C10 film can rotate from (113) through other orientations before the peaks disappear. Finally, the SO_3 films have been previously observed to nucleate with the [106] axis along the surface normal.[1] The (106) peak is absent in the calcite spectrum, but when examining the diffraction pattern along the surface normal we found numerous (116) and (006) peaks, which are tilted about 30° away from the [106] axis. This again shows the degree of variation in orientation of the preferred planes. By tilting the sample goniometer to the appropriate angle, we confirmed that SO_3-nucleated crystals were primarily (106) oriented (data not shown). Once more, the preferred orientation is only dominant for $n < 2$.

D. Lattice Parameters and Mg Incorporation. To determine the crystal structures of these sparse coatings of microparticles, we took scans with the beam lying within the plane of the films. These data therefore reflect *d* spacings parallel to that plane. Strong Bragg peaks observed for all samples indicate that the calcite is crystalline, at least by the time of the measurements conducted some months after synthesis and storage in air (Figure 4). The relative intensities of peaks reflect the preferential orientation toward the surface normal. The in-plane X-ray diffraction patterns of calcite without Mg^{2+}, shown at the bottom of each panel in Figure 4, have different missing peaks corresponding to the orientational order. However, when Mg^{2+} incorporation into calcite increases, the data more closely resemble the calcite powder pattern, no matter what kind of functional group or chain length of SAM. These data show that the spherical particles in the SEM images are randomly oriented calcite crystals.

The peaks broaden, split, and shift to higher 2θ value as *n* increases, as shown in Figure 5. Only sharp peaks ($<0.1°$ in 2θ) are obtained for $n = 0$. The broadest peaks of $0.3-0.4°$ in 2θ are obtained above $n = 2$. At intermediate Mg concentrations, the splittings of peaks are observed ($n = 0.5-1.5$), with the broader one being shifted to higher angle in 2θ. This means that two Mg calcite phases of distinct composition coexist in the films, for all these SAMs studied. In the case of SO3 film, where our micrographs show three different orientations for $n \leq 1$, one might presume that the Mg incorporation could differ between them. However, since SEM micrographs show only one crystal morphology for $n = 0.5$ and $n = 1.0$ for C15 and C10 films, the two phases evidently can exhibit the same preferred orientation despite differences in the lattice parameter. We attempted to distinguish Mg content in particular crystals using EDS in the electron microscope, but this method was not sensitive enough to obtain any other information. Therefore, no obvious dependence on the choice of surfactant is observed regarding the two-phase coexistence.

According to the calculated lattice parameters, Mg^{2+} incorporation shrinks the calcite lattice by a few percent ($\Delta a \approx 1.5\%$ and $\Delta c \approx 2.0\%$). Lattice parameters and cell volumes obtained from the data are shown in Figure 6. Where enough split peaks could be distinguished, we plot additional symbols (in $n = 0.5, 1.0$) for the two distinct Mg calcite phases. Comparison to geological magnesian calcite literature suggests that Mg incorporation reaches a value of 18 mol % for the $n = 4$ films.[7] Here, we could not find any dependence on the differently functionalized alkanethiols.

IV. Discussion

High-resolution measurements present a new picture of the texture and orientation of SAM-nucleated magnesian calcites. Figure 7 shows how the film is built up, and how the angular spreads and coherence lengths of each layer differ from each other. We determined coherence lengths in ranges for each film component, on the basis of average peak widths and the simplest version of the Scherrer equation.

First is the silicon wafer, which is essentially a perfect single crystal and shows that coherence lengths up to 300 nm can be measured. On the thin Ti metal bonding layer (too thin to be measured well by X-rays), the Au film crystallinity is broken up into domains of ~18 nm in all directions. This should not be confused with the macroscopic film thickness of 500 nm. The angular spread of the Au [111] axis is distributed through 2.6° about the surface normal. The SAM is too disordered to be seen, evidently because of substrate roughness. We estimate that the surfactant molecules are ordered only on 1−10 nm coherence lengths. The tilt of the hydrocarbon tails is unknown: it is possible that the vacuum structure[18] may be rearranged by exposure to ions in solution. At any rate, the SAM domains must be at least as disordered as the Au in terms of relative angular spreads.

For samples without Mg, calcite is observed as individual crystals which are oriented with equal probability in the range ±6° about the surface normal. This is distinctly different from the smoothly varying orientation of the Au [111] axis. Even faceting the nucleated planes would not result in good contact between the calcite and SAM. Previous work by Han, Aizenberg, Black, and Whitesides[14,15] showed that the preferred orientation of calcite followed a pattern of matching the carbonate group tilt to the presumed alignment of the SAM carboxylic group. However, the present coherence length measurements show that this stereochemical alignment could not extend throughout an entire crystal interface. Although the calcite crystals range from 1 to 20 μm in size, the peaks are broadened compared to the

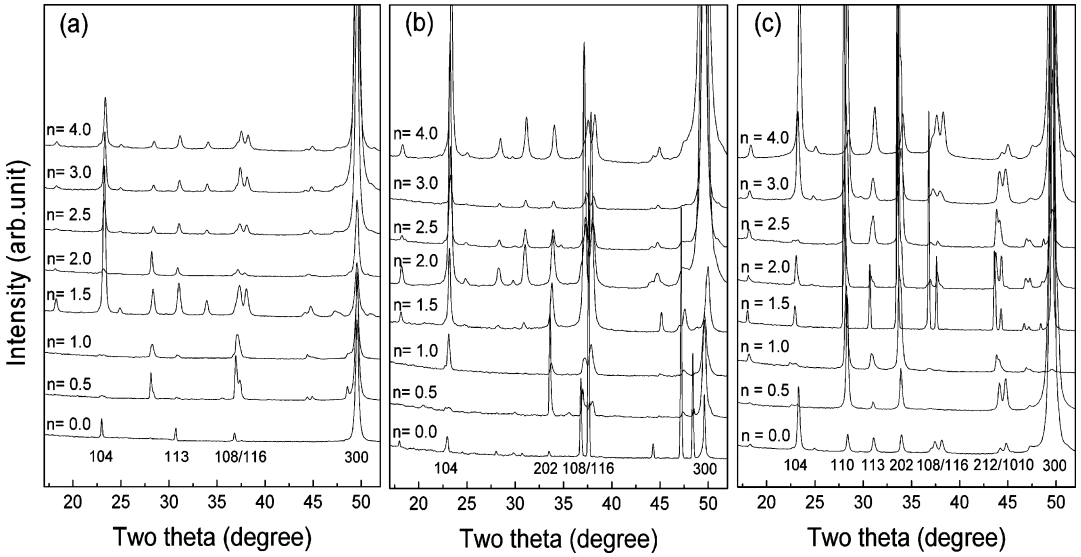

Figure 4. 2θ scans showing all peaks lying within the plane of the film: (a) C15 film; (b) C10 film; and (c) SO_3 film. Each panel shows all samples for $n = 0.0-4.0$.

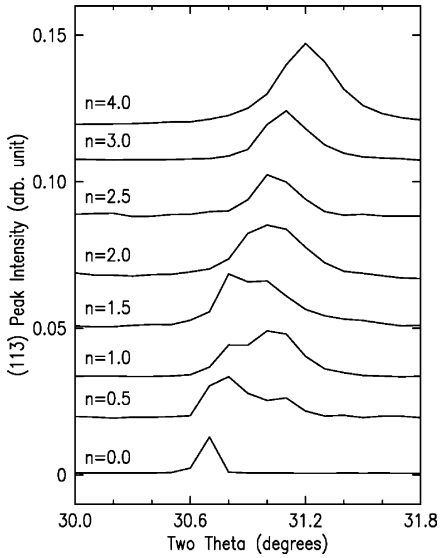

Figure 5. The (113) peaks of calcite on SO3 films for each n value.

silicon, and coherence lengths of only 90−125 nm are indicated by the data. This is still larger than any given domain in the SAM or the Au (18 nm). The SAM structure presumably affects the calcite nuclei only at extremely early times, at small, localized nucleation sites.

At the upper limit of Mg incorporation, all mineral particles are spherical and show no preferred orientation. Their coherence lengths are smaller still, on the order of 12−25 nm. Again, these coherent domains are much smaller than the particles themselves, which reach 2 μm in size. For these crystals, the spherical shape results from an amorphous precursor phase. X-ray measurements were performed after some months of storage in air, and so the amorphous structure factors of these particles have not been measured experimentally. We presume that these samples crystallized relatively quickly after being removed from solution. X-ray measurements were taken 3, 6, and 10 months later, and each study found the same peak widths; thus, no long-term crystallization process is indicated. Dehydration allows such particles to crystallize, and when it does, waters of hydration must exit the particle, and this disrupts crystal grains. This explanation is probably enough to account for the very small coherence lengths. Mg incorporation determined from the analysis of lattice parameters shows that the same limit of 18 mol % Mg is reached, regardless of SAM type.

With this last piece of information, we can complete our description of Mg calcite nucleation in this system. Our experimental procedure appears to allow two routes to magnesian calcite mineralization. The first is favored for low Mg concentrations and typified when $n = 0$. The choice of surfactant can control which calcite face may be stabilized against the SAM. These crystals continue to express (104) faces toward the solution. They can incorporate Mg up to concentrations of ~8 mol %. The main difference between SAMs is that they release the oriented calcite crystals at slightly different Mg levels. This is expected, since the interaction with Mg is different for different calcite faces.[19] The second route, dominating for $n = 4$, produces spherical particles, through an amorphous precursor phase. The composition indicated by lattice parameters is 18 mol %, and there is no evidence that the SAM affects their growth directly. In our experiments, the samples with $0 < n < 4$ show coexistence of both of these phases, most clearly in the synchrotron X-ray diffraction patterns. This tells us that the solution concentration of Mg alone cannot quantitatively dictate Mg incorporation into calcite. Even at $n = 0.5$ the amorphous precursor route with ~18 mol % exists: however, it does not outcompete oriented growth until the Mg content reaches $n = 2$. Therefore, the SAM has a very clear role in preferentially nucleating the low-Mg phases and stabilizing them under conditions where a high-Mg phase is otherwise more favorable.

There are two obvious routes for future studies to improve our knowledge of the organic/mineral even further. The first involves control of the mineralization conditions. It is recognized that the gas-diffusion synthesis method is one which scans the saturation as a function of time. This time scale is convolved with other time scales for mineralization, making it questionable to interpret the kinetics or to extend the conclusions

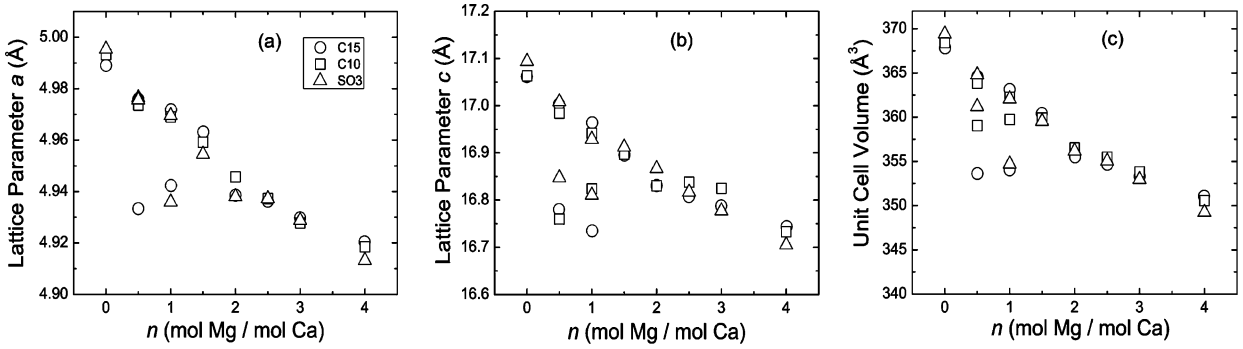

Figure 6. Plots of (a) the lattice parameter a for calcites, (b) the lattice parameter c for calcites, and (c) the unit cell volume for calcites on each functionalized SAM as a function of the Mg concentration in solution.

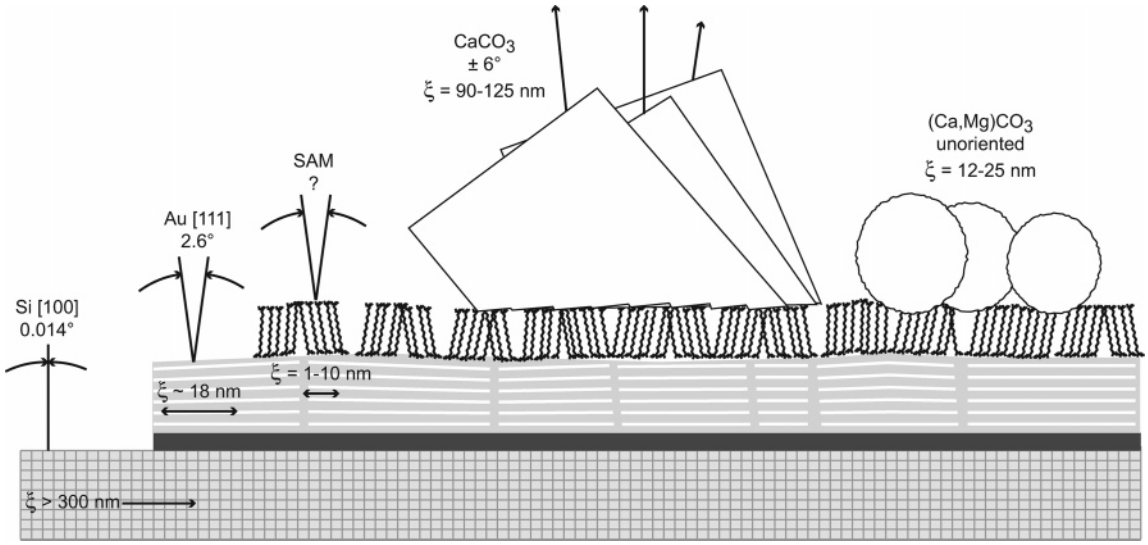

Figure 7. Schematic illustration of film buildup and angular spreads and coherence lengths on each layer.

when conditions differ from one experiment to another. In fact, in situ X-ray studies have already demonstrated that vaterite versus calcite can be selected by solution conditions, while nucleating against fatty acid films with identical structures.[20] Interpretations of calcium carbonate nucleation are more meaningful when the saturation is controlled, as others in the literature have demonstrated.[7,12,21] This point is important for both biological and geological interpretations: especially since the Mg calcite nucleation (oriented by the SAM) and growth (affected strongly by Mg) are coupled, as shown by the fact that differential Mg incorporation can occur when an organic film is present. A flow cell for closed-system $CaCO_3$ mineralization is under development at BNL for future studies. A second point is that in this study as many crystallites as possible were placed into the illuminated beam path, so that we could obtain a good statistical average of the orientations and coherence lengths produced under our systematically varied conditions. Having reached this point, it would now be desirable to correlate these orientations for each crystallite independently and to learn more about the lateral correlations as well. The synchrotron X-ray microbeam is capable of bridging the length scales between bulk X-ray diffraction and electron microscopy in just this way. The micrometer-scale crystals achieved by nucleating on SAMs are very well matched to the micrometer spot sizes currently available, and we look forward to future work in this direction.

V. Summary

In summary, we have investigated nucleation of Mg calcite by functionalized alkanethiol self-assembled monolayers (SAMs). The distinct preferred orientation of calcite crystals is predominant for solution $[Mg^{2+}]/[Ca^{2+}]$ ratios from 0.5 to 2.0, depending on SAM type. These crystals incorporate Mg up to at least 8 mol %. At high $[Mg^{2+}]/[Ca^{2+}]$ solution ratios of 2.0−4.0, spherical, polycrystalline Mg calcite particles are induced, with 10−18 mol % Mg, as determined from X-ray diffraction. Our results suggest two paths to Mg calcite morphogenesis: one in which the development of an oriented crystalline phase dependent on an organic interface occurs and the other high-Mg phase mediated by an amorphous precursor independent of an organic interface. Even under similar solution conditions, Mg incorporation into crystals can differ from that into amorphous calcium carbonate.

Acknowledgment. This manuscript has been authored by Brookhaven Science Associates, LLC, under Contract No. DE-AC02-98CH10886 and The Advanced Photon Source under Contract No. W-31-109-Eng-38 with the U.S. Department of Energy. The United States Government retains, and the publisher, by accepting the article for publication, acknowledges, a worldwide license to publish or reproduce the published form of this manuscript, or allow others to do so, for United States Government purposes.

Supporting Information Available: Results of synchrotron X-ray reflectivity and grazing incidence X-ray diffraction from unmineralized C10 and C15 SAMs on E-beam evaporated Au (111) substrates. This material is available free of charge via the Internet at http://pubs.acs.org.

References

(1) Han, Y.-J.; Wysocki, L. M.; Thanawala, M. S.; Siegrist, T.; Aizenberg, J. *Angew. Chem., Int. Ed.* **2005**, *117*, 2438.
(2) Russell, A. D.; Hönisch, B.; Spero, H. J.; Lea, D. W. *Geochim. Cosmochim. Acta* **2004**, *68*, 4347.
(3) Chang, V. T.-C.; Williams, R. J. P.; Makishima, A.; Belshawl, N. S.; O'Nions, R. K. *Biochem. Biophys. Res. Commun.* **2004**, *323*, 79.
(4) Lear, C. H.; Rosenthal, Y.; Slowey, N. *Geochim. Cosmochim. Acta* **2002**, *66*, 3375.
(5) Beck, L.; Bassinot, F.; Gehlen, M.; Trouslard, Ph.; Pellegrino, S.; Levi, C. *Nucl. Instrum. Methods Phys. Res. B* **2002**, *190*, 482.
(6) Stanley, S. M.; Ries, J. B.; Hardie, L. A. *Proc. Natl. Acad. Sci. U.S.A.* **2002**, *99*, 15323.
(7) Reeder, R. J. *Carbonates: Mineralogy and Chemistry*; Reviews in Mineralogy 11; Mineralogy Society of America, BookCrafters Inc.: Chelsea, MI, 1990.
(8) Chen, T.; Neville, A.; Yuan, M. *J. Cryst. Growth* **2005**, *275*, e1341.
(9) Jimenez-Lopez, C.; Rodriguez-Navarro, A.; Dominguez-Vera, J. M.; Garcia-Ruiz, J. M. *Geochim. Cosmochim. Acta* **2003**, *67*, 1667.
(10) Titiloye, J. O.; de Leeuw, N. H.; Parker, S. C. *Geochim. Cosmochim. Acta* **1998**, *62*, 2637.
(11) Paquette, J.; Reeder, R. J. *Geology* **1990**, *18*, 1244.
(12) Davis, K. J.; Dove, P. M.; Wasylenki, L. E.; De Yoreo, J. J. *Am. Mineral.* **2004**, *89*, 714.
(13) Travaille, A. M.; Kaptijn, L.; Verwer, P.; Hulsken, B.; Elemans, J. A. A. W.; Nolte, R. J. M.; van Kempen, H. *J. Am. Chem. Soc.* **2003**, *125*, 11571.
(14) Aizenberg, J.; Black, A. J.; Whitesides, G. M. *Nature* **1999**, *398*, 495.
(15) Han, Y.-J.; Aizenberg, J. *J. Am. Chem. Soc.* **2003**, *125*, 4032.
(16) Han, Y.-J.; Aizenberg, J. *Angew. Chem.* **2003**, *42*, 3668.
(17) Li, J.; Liang, K. S.; Scoles, G.; Ulman, A. *Langmuir* **1995**, *11*, 4427.
(18) Love, J. C.; Estroff, L. A.; Kriebel, J. K.; Nuzzo, R. G.; Whitesides, G. M. *Chem. Rev.* **2005**, *105*, 1103.
(19) Paquette, J.; Reeder, R. J. *Geochim. Cosmochim. Acta* **1995**, *59*, 735.
(20) DiMasi, E.; Olszta, M. J.; Patel, V. M.; Gower, L. B. *Cryst. Eng. Commun.* **2003**, *5*, 346.
(21) Travaille, A. M.; Steijven, E. G. A.; Meekes, H.; van Kempen, H. *J. Phys. Chem. B* **2005**, *109*, 5618.

CG050164X